Accelerating Shock-Driven Reactions in Metal Nanocomposites

Siva Kumar Valluri[1, a)], Edward L. Dreizin [2)] and Dana D. Dlott[1]
[1]*School of Chemical Sciences and Fredrick E. Seitz Materials Research Laboratory, Box 01-6 CLSL, 600 S. Goodwin Ave., Urbana, IL 61801, USA*
[2]*Otto H. York Department of Chemical and Materials Engineering, New Jersey Institute of Technology, University Heights, Newark, New Jersey 07102*

[a)] Corresponding author: svalluri@illinois.edu

Abstract. Metal powders are sought as energetic additives to conventional explosives. However, due to their sluggish reaction kinetics with external gaseous oxidizers, pure metals are replaced with metallic composites with intimately mixed condensed phase oxidizers prepared by arrested reactive milling (ARM). Such composites can be initiated by non-thermal, mechanical means; through shear mixing of fuel and oxidizer under a shock compressive load. Since the ARM preparatory technique allows for tuning multiple powder attributes such as fuel/oxidizer of interest, their degree of mixing, amount of oxidizer, particle porosity, among others, a parametric study is crucial in identifying suitable traits for fast reactions in metal composites. Using our high-throughput benchtop experimentation we deliver shocks to isolated powder particles suspended in transparent polymer by impacting them with laser driven flyer plates. The emission from the shock compressed particles is followed using an optical emission pyrometer as well as a high-speed camera to follow evolution of reactivity in individual particles. In this manner a variety of samples can be tested quickly to explore the parametric space. In recent work, to probe the role of porosity, porous Al-MoO3-KNO3 prepared by milling in a hexane acetonitrile emulsion was shock compressed. In particles where sufficiently large pores over 2μm were identified, shock-initiation was achieved consistently. In this work, the same composite powder's reactive behavior was characterized to judge the improvement in pore collapse-driven ignition and subsequent combustion kinetics. When compared to Octogen's (HMX) deflagration under the same experimental conditions, the composite was found to have equally fast hotspot formation and onset of redox reaction within nanoseconds of HMX. Using intensities of emission plumes observed within particles as proxy for temperatures, we find that even larger porous particles with poor surface area to volume ratio showed fast rise in temperature. This is suggested to be due to the more effective mixing of fuel-oxidizer laminates in large particles that have a higher number of pores and larger sized pores.

INTRODUCTION

Aluminum powder has long been considered as an additive in conventional CHNO explosives to increase energy density [1-4] and improve detonation characteristics, such as overpressure. The transport-limited reaction of micron-sized metal powders with external gaseous oxidizers results in a delayed ignition onset of several microseconds [5] and sluggish combustion spanning microseconds [6, 7], even in extreme conditions observed during detonations [8-10]. This limits the energy release to afterburn, behind the fast detonation reaction zone spanning nanoseconds. To enhance the combustion kinetics of metallic additives, composites formed by intimately mixing condensed phase oxidizers with aluminum using arrested reactive milling (ARM) are considered as alternatives. Preliminary exploration involving the shocking of individual fuel-rich Al-MoO3 ARM composite particles showed a promising improvement in ignition delay presenting the possibility of shear-mixed reactions [11]. Given that multiple powder attributes can impact shock sensitivity, such as the choice of oxidizer, mass fraction of oxidizer, degree of mixing between oxidizer and aluminum, porosity, among others, this creates a parametric space for designing suitable additives. We have designed a high-throughput tabletop experimentation using laser-driven flyer plates to deliver shocks to isolated particles and characterize their emissions to quantify the role of each powder attribute [12].

As an initial step, recent work introduced internal pores to sensitize isolated particles [13]. The particle porosity was adjustable using a technique involving milling in an emulsion of hexane as the continuous phase and acetonitrile as the droplet phase [14]. When sufficiently large pores were present, Al-MoO3-KNO3 particles were found to emit during the short duration shock itself [13]. In the current study, we investigate the efficacy of particle porosity in igniting and combusting the composite particle during the deflagration timescales observed in explosives. We employ laser-launched flyer plates to deliver short duration shocks, and we characterize the thermal emissions from isolated composite particles suspended in transparent polymer. Additionally, the high-speed video enables us to follow reactivity of individual particles with nanosecond temporal resolution. These results will be compared with Octogen (HMX) tested in the exact same manner, serving as a benchmark.

EXPERIMENTAL

The porous powder, referred to as the composite, consisting of Al-MoO3-KNO3, was tested in this study. Details regarding the preparation of the composite and the characterization of powder properties have been documented in a previous work [13]. Figure 1 illustrates the observed pore sizes within composite particles as a function of their size [13], along with the ratio of particle surface area to its volume calculated as if the particle were spherical. Owing to the nature of composite preparation, the pore size distribution and number density within the composite particle increases with its size. This results in a scenario where size dependent behavior is expected.

The HMX crystals were extracted from a commercial source, N-5 explosive by dissolving it in acetone and recrystallizing, to obtain a repeatable size and morphology that is described in [15].

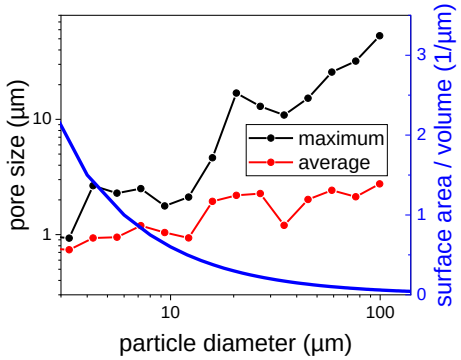

FIGURE 1. The average and maximum pore sizes observed in the cross-sections of Al-MoO_3-KNO_3 composite particles imaged using a scanning electron microscope (taken from [13]) along with the ratio of particle surface area to its volume calculated as if the particle were spherical and plotted as a function of size.

To evaluate the shock compression-triggered reactive behavior of both the composite and HMX samples, we suspended them in transparent polydimethylsiloxane (PDMS) polymer that allows us to see every particle during shock. Figure 2a illustrates the experimental setup. The composite particles were dispersed in PDMS within 250 μm deep wells with 3 mm diameters, that were milled into Teflon sheets and mounted onto glass substrates. Each target contained 92 wells, allowing for high-throughput experimentation. HMX crystals were suspended in PDMS and spin-coated into 45 μm thick layers directly onto the glass substrates. The HMX crystals tended to agglomerate in PDMS to form clusters whose size distribution was comparable to that of the composite powder. An additional baseline sample of pure PDMS filled into the Teflon wells were also tested to characterize the behavior of the polymer devoid of energetic inclusions. This is because the polymer is capable of reactive behavior due to cross-linking catalysts present in it. The shock was delivered by impact using a circular aluminum 1101 foil, measuring 500 μm in diameter and 25 μm thick, which was punched out by a flat-topped laser pulse with a pre-determined energy. The laser energy was carefully attenuated to achieve the intended terminal velocity of the flyer, which was set at 4 km/s for all measurements in this study to maintain a consistent perturbation. Experimental velocity variations between runs remained within 0.1 km/s.

As depicted in Figure 2a, optical access at the bottom of both sample targets allowed for visible light pyrometry and high-speed imaging using a 4-frame SIMX camera with a spatial resolution of 3 μm and a temporal resolution of 3 ns. A calibrated 32-channel fast spectrometer was used to measure spectral radiance from 0.8 ns to 120 μs, served as our pyrometer. To ensure consistency across measurements, a spherically integrated tungsten lamp was used for calibration purposes [16]. The experimental setup employed in this study, along with the instrumental settings, is comprehensively described in [13] and has been adapted from the setup used for studying single HMX crystals [17].

Figure 2b presents the output of the optical pyrometer obtained from a typical shock compression run in the form of spectrally integrated spectral radiance and temperatures derived by fitting the spectral intensities using a gray-body assumption. Time zero is defined as the moment when the flyer impacts the sample surface. The radiance curves of the composite were normalized based on the particle occlusion observed by the SIMX camera to enable a fair comparison with the HMX benchmark. As seen in Figure 2c-2g, the images captured by the SIMX camera include a stationary back-lit image acquired before the shock experiment, which helps identify particle locations (Figure 2c), and four emission frames (Figure 2d-2g) taken after the flyer impact. By appropriately setting the delay and exposures on the SIMX camera frames, we observed the time intervals of 0-40 ns to capture emissions during the initial shock transit and three subsequent frames spanning 80-130 ns, 180 230 ns, and 230-380 ns to track emissions.

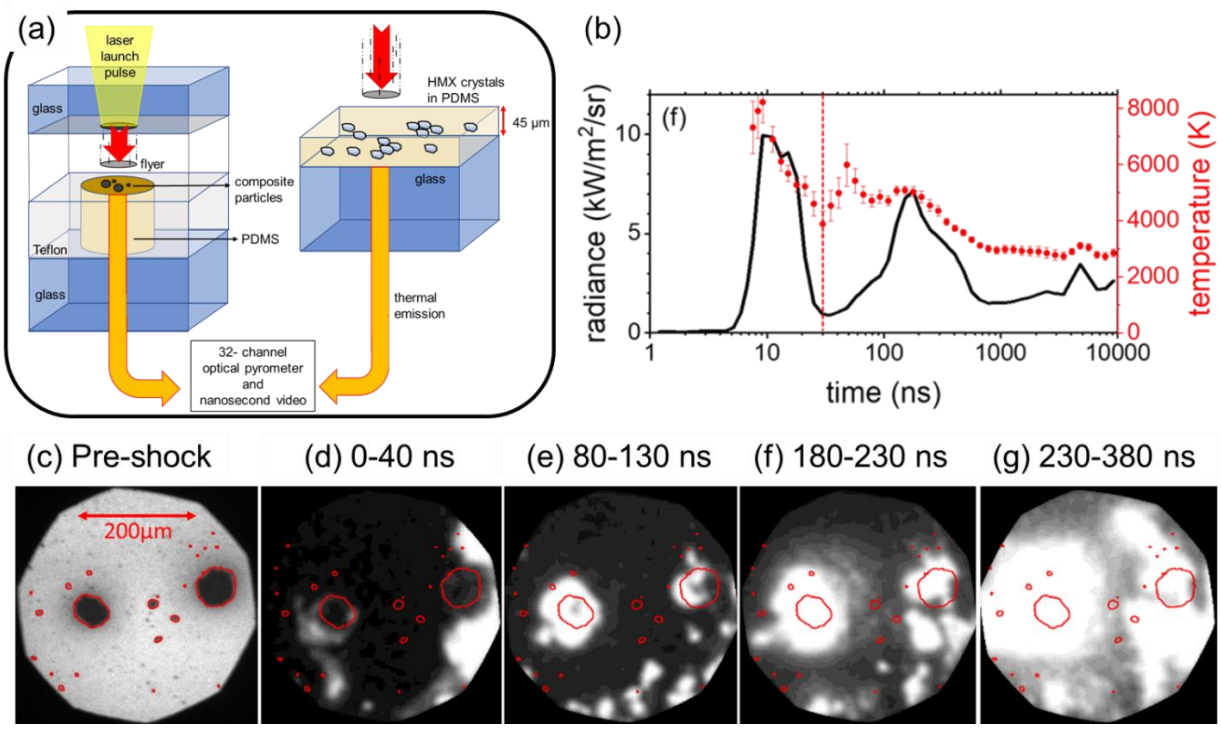

FIGURE 2. (a) The experimental schematics for shocking dispersed Al-MoO3-KNO3 composite particles in PDMS wells 250 μm deep and HMX particle clusters in PDMS spin coated over glass into 45 μm thick layers. The particle occlusion of the field-of-view across all runs for both the composite particles and HMX benchmark are similar to enable comparison. Typical (b) spectrally integrated radiance and gray body temperatures of a shock compression run, and corresponding (c-g) images captured by the high-speed camera when Al-MoO3-KNO3 particles were tested. The SIMX camera yields (c) a backlit image obtained before the shock experiment and four frames of emissions observed after flyer impact where moment of impact is taken as time zero: (d) 0-40 ns, (e) 80-130 ns, (f) 180-230 ns, and (g) 230-280 ns. The particle boundaries obtained from pre-shock image (c) are over laid on subsequent emission frames (d-g) as red lines to allow for spatial tracking of emission seen as bright pixels on a dark background.

By utilizing a custom Python code, we segmented the pre-shock stationary images (e.g., Figure 2c) to identify particle regions and spatially designate emissions. Assuming minimal particle movement in the plane during shock transit, we overlaid subsequent emission frames with particle boundaries identified (visible as red lines in Figure 2c-2g) to track emissions within particles. We collected pixel intensities within each region associated with a particle across the frames of observation to quantify emission growth as a function of time and particle size.

RESULTS AND DISCUSSION

The optical pyrometer data, comprising spectrally integrated radiance and gray-body temperatures, are presented in Figures 3a and 3b, respectively, for composite and HMX clusters suspended in PDMS, along with pure PDMS serving as a baseline. Both radiance and temperatures presented have been averaged across multiple runs, capturing details of over 2000 composite particles and 500 clusters in the case of HMX.

As shown in Figure 3a, the radiance traces of all three tested materials exhibit two humps, one appearing a few nanoseconds after impact and the other occurring much later. The features resembling multiple peaks in the second hump result from averaging across multiple particles/clusters with different material characteristics, and hence, burn characteristics. Notably, the radiance intensities of both the composite and HMX, as seen in Figure 3a, are significantly stronger than for pure PDMS. The rise in radiance of the initial peak in the nanoseconds is associated with the passage of the shock, leading to the formation of several hotspots due to gas compression in pores and shear mixing of aluminum and oxidizer layers in the composites. In the HMX sample, this rise is attributed to hotspots formed due to shear-driven deformation of microstructure in clusters. After the shock departs from the sample, the radiance decays due to the quenching of most hotspots, leaving only the 'critical hotspots' with sufficiently large thermal mass and reasonably high temperature to ignite the sample through material chemistry [18]. The saddle point after which the radiance grows into the second hump is interpreted as the coalescence of critical hotspots to initiate

combustion of the composite particles and deflagration in the case of HMX clusters. The time delay in hotspot formation in the samples is denoted by the initial peak position. As seen in Figure 3a, the 9 ns delay in hotspot formation in composite porous particles is within nanoseconds of HMX clusters (5 ns delay). Considering the variations in particle embedding depth beneath polymer surface and experimental error of 5ns, this observed difference is trivial. The saddle point, indicating the onset of material chemistry for both the composite and HMX, is comparable at around 40 ns. As sufficient time progresses, heat generation becomes dominant and reaction fronts form. As nearly a microsecond passes, apart from the development of combustion/deflagration fronts within particles/ clusters, due to heat and mass exchange between particles and polymer, side reactions with polymer are also possible. The behavior of pure PDMS is hence presented as baseline as seen in Figure 3a. Pure PDMS shows a diminished radiance trace overall. The feeble nanosecond peak observed is attributable to the collapse of gas bubbles trapped in the polymer during shock transit. The subsequent increase in radiance is due to local reaction of the polymer with metallic catalysts added for cross-linking which is energetically weaker than combustion / deflagration dominated reactions observed in the composite and HMX samples. The integral of the radiance curve, with units J/Sr.m², represents the energy emitted by the samples. The observed energy emitted by the opaque composite particles (1.13x107 J/Sr•m²), while not in its entirety, is still comparable to that of the optically transparent HMX clusters (6.45x106 J/Sr•m²) across the observation window from 1 ns to 10 μs after impact. The reaction in HMX clusters is nearly completed by the end of the observation window while composite combustion is ongoing as evidenced by the decay of the radiance curve of HMX to the range of pure PDMS while composite radiance is stronger.

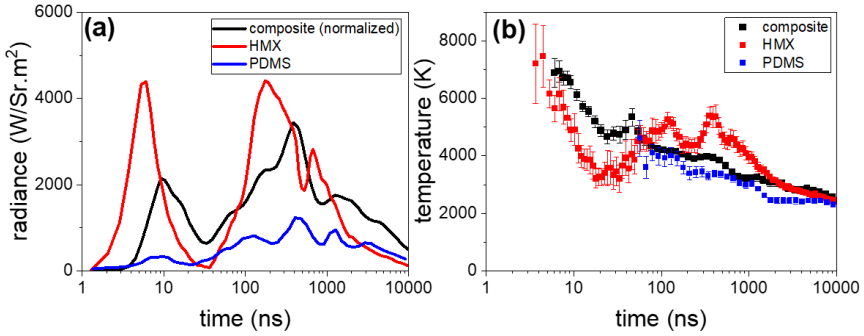

FIGURE 3. The optical emission pyrometry data of shock compressed Al-MoO3-KNO3 composite particles and HMX clusters suspended in PDMS along with pure PDMS: (a) The averaged radiance traces of samples along with their corresponding (b) averaged graybody temperatures over the same observation period. The error bars in the temperature plot represent the 90 % confidence intervals. The radiance trace of the composite particles is normalized by a factor of 0.7 to be comparable to the more sparsely distributed HMX clusters to equate the occlusion of field-of-view by dispersed particles/clusters. The gray-body temperatures presented are biased towards the hottest temperatures in the field of view at the instance of observation.

In Figure 3b, the gray-body temperatures of the samples, which are biased toward the hottest temperatures in the field of view, are interpreted as hotspot temperatures during the initial moments after impact. The temperatures observed in both the composite and the HMX reference are significantly hotter than expected deflagration temperatures, around 7000K, suggesting gas compression within voids/pores [19]. These hotspots subsequently cool by losing heat radiatively and through heat transfer to surrounding matter until material decomposition in the case of HMX and thermite reactions in the composite become energetically dominant. At this point, the temperature decrease is arrested, as shown in Figure 3b, and the hottest region in the field of view becomes the ignited portion of the sample. Figure 3b also indicates that the instance of material chemistry becoming significant for the composite and HMX is comparable ~20 ns. The temperatures of the samples tested gradually drop as combustion / deflagration events consume the particles / clusters. The gray-body temperatures collected in the case of PDMS show the low-concentration but energetic metal-polymer chain reactions resulting in the measured temperatures being nearly comparable to the composite combustion as seen in Figure 3b. However, this is a collection of localized events of low thermal mass as evidenced by the diminished radiance trace seen in Figure 3a.

Through the emission frames captured by the high-speed camera, we can observe the growth in emission plumes and indirectly track the rise in their temperatures by measuring the spatial intensities within regions associated with specific particles since intensity is proportional to temperature raised to a power four. As the temperatures obtained by the pyrometer are skewed towards the hottest areas in the field-of-view, we can use the emission frames to quantify the range of intensities observed and hence estimate the spatially averaged temperatures within regions of interest. Figure 4a demonstrates how the particle boundaries obtained from the pre-shock stationary image (like Figure 2c) are overlaid onto convolution smoothed emission frames to spatially allocate emissions. The pixel intensities within the particles are collected over successive emission frames

to track emissions. Since the sizing of the identified particles is also possible, the distribution of pixel intensities within the particles is plotted (as box plots) as a function of its size over the four instances of observation, as seen in Figure 4b-4e: 4b (20 ± 20 ns), 4c (105 ± 25 ns), 4d (205 ± 25 ns), and 4e (305 ± 75 ns).

As evident from Figures 4b-4e, the mean intensities within particles collectively exhibit a steady rise across all sizes, starting from 20 ns and continuing until 305 ns, at which point the intensities become approximately four times stronger. Consequently, the mean temperatures within particles are estimated to be 1.4 times hotter. If we were to assume that the shear-mixing enhanced by hydrodynamic pore collapse was ineffective, the conventional shear-initiated and thermally stimulated reactions would become the dominant mechanisms. Since the degree of mixing is comparable across sizes, we would expect the smaller less porous particles, with their significantly higher surface area to volume ratio (see Figure 1), to display a faster increase in temperature (and consequently, pixel intensity) due to quicker heat transfer within particle and with polymer matrix. However, our initial observations seen in Figures 4b and 4c show larger particles with more pronounced porosity in the form of large pores (as shown in Figure 1) exhibit a swifter rise in intensities. This suggests the role of increased efficiency of pore collapse in large particles initiating the mixing of fuel-oxidizer layers, as predicted by Zhao et al. in porous Al-Ni laminate systems [20]. It's important to note that the role of particle size cannot be separated from this observation, as larger particles are also more susceptible to deformation under compressive forces. By 305 ns, when thermal diffusion has sufficiently progressed, nearly all particles, both small and large, exhibit significantly intense pixels, as seen in Figure 4e.

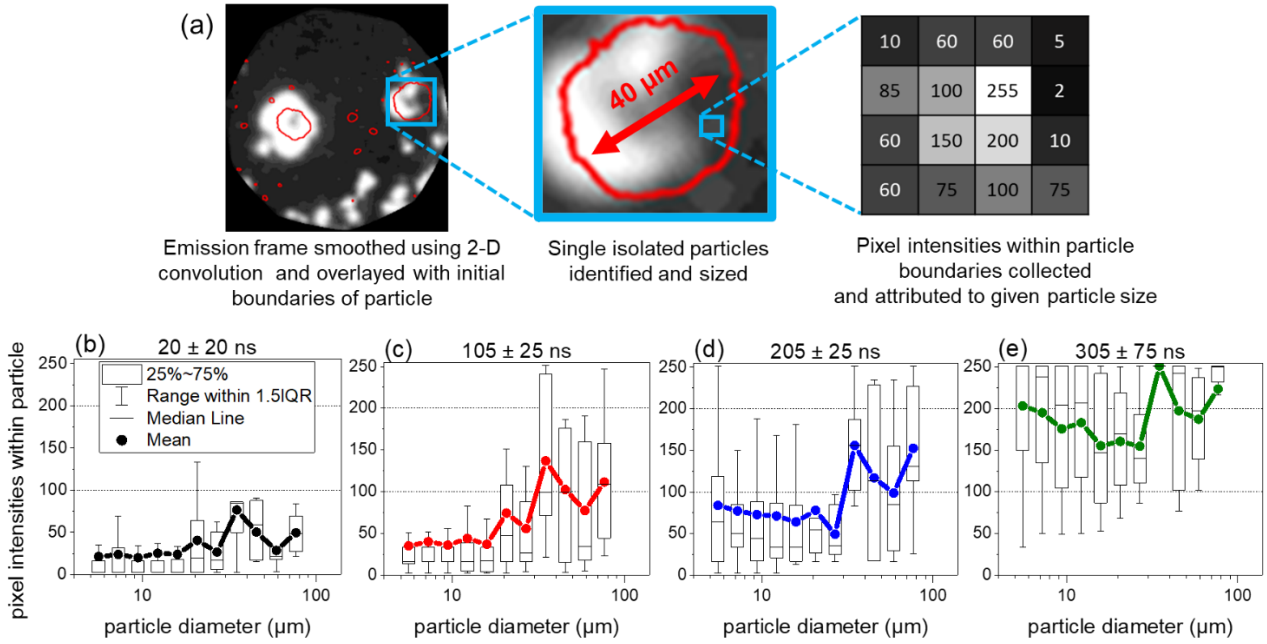

FIGURE 4. (a) Illustration showing the steps involved in obtaining pixel intensities within the expected boundaries of a particle at a given instance of observation. (b-e) The distribution of pixel intensities within Al-MoO3-KNO3 composite particles as a function of their size, observed at various instances after flyer impact; (b) 20 ± 20 ns, (c) 105 ± 25 ns, (d) 205 ± 25 ns, and (e) 305 ± 75 ns. The error bars on time are a consequence of exposure settings employed for each frame: (a) 40ns, (b) 50ns, (c) 50ns, and (d) 150 ns. The distributions of pixel intensities are presented as box plots whose attributes can be seen in the legend shown in (b). The mean pixel intensities within a particle of a given size are connected by a bold line to its neighbors. Horizontal lines at 100- and 200-pixel intensities are provided as visual guides to track rise in pixel intensities with time.

CONCLUSIONS

The porous Al-MoO3-KNO3 composite particles exhibit an accelerated reaction onset and combustion attributed to the enhanced shear mixing facilitated by the hydrodynamic pore collapse when subjected to suitably strong shock. Notably, the formation of hotspots due to pore collapse was observed as early as 9 ns after the impact of the flyer. This observation aligns with the heat generation indicative of material chemistry becoming dominant after shock compression, and it is comparable to the behavior seen in the case of HMX. The overall rise in particle temperatures is expected due to shear-initiated thermite reactions within, as evidenced by the increase in spatially allocated emission intensities. Moreover, porosity may play a role in kinetically improving reactions in larger particles.

ACKNOWLEDGMENTS

The research at University of Illinois, Urbana-Champaign was supported by the US Army Research Office under awards W911NF-19-2-0037 and W911NF-16-1-0406 and at New Jersey Institute of Technology by the US Defense Threat Reduction Agency under the award HDTRA12020001/2004756624, and by the US Office of Naval Research under the award N00014-19-1-2048. The characterization of the prepared composites was carried out in part in the Materials Research Laboratory Central Research Facilities, University of Illinois.

REFERENCES

1. Yetter, R.A., G.A. Risha, and S.F. Son, Metal particle combustion and nanotechnology. Proceedings of the Combustion Institute, 2009. 32 II: p. 1819-1838.
2. Dreizin, E.L., Metal-based reactive nanomaterials. Progress in Energy and Combustion Science, 2009. 35(2): p. 141-167.
3. Gany, A. and D.W. Netzer, Combustion studies of metallized fuels for solid-fuel ramjets. Journal of Propulsion and Power, 1986. 2(5): p. 423-427.
4. Sundaram, D., V. Yang, and R.A. Yetter, Metal-based nanoenergetic materials: Synthesis, properties, and applications. Progress in Energy and Combustion Science, 2017. 61: p. 293-365.
5. Glassman, I., R.A. Yetter, and N.G. Glumac, Combustion. 2014: Academic press.
6. Corcoran, A.L., V.K. Hoffmann, and E.L. Dreizin, Aluminum particle combustion in turbulent flames. Combustion and Flame, 2013. 160(3): p. 718-724.
7. Mohan, S., L. Furet, and E.L. Dreizin, Aluminum particle ignition in different oxidizing environments. Combustion and Flame, 2010. 157(7): p. 1356-1363.
8. Peuker, J.M., H. Krier, and N. Glumac, Particle size and gas environment effects on blast and overpressure enhancement in aluminized explosives. Proceedings of the Combustion Institute, 2013. 34(2): p. 2205-2212.
9. Trzciński, W.A., S. Cudzilo, and L. Szymańczyk, Studies of detonation characteristics of aluminum enriched RDX compositions. Propellants, Explosives, Pyrotechnics, 2007. 32(5): p. 392-400.
10. Bazyn, T., H. Krier, and N. Glumac, Oxidizer and pressure effects on the combustion of 10-μm aluminum particles. Journal of Propulsion and Power, 2005. 21(4): p. 577-582.
11. Shaw, W.L., et al., Ignition of Nanocomposite Thermites by Electric Spark and Shock Wave. Propellants, Explosives, Pyrotechnics, 2014. 39(3): p. 444-453.
12. Kumar Valluri, S., et al., Fast reactions of shocked energetic microporous metallic composites. Propellants, Explosives, Pyrotechnics, 2023. 48(10): p. e202300031.
13. Valluri, S.K., E.L. Dreizin, and D.D. Dlott, Porosity: The key to initiating metallic composite particles under shock compression. AIP Conference Proceedings, 2023. 2844(1).
14. Mursalat, M., et al., Microspheres with Diverse Material Compositions Can be Prepared by Mechanical Milling. Advanced Engineering Materials, 2020. 22(3): p. 1901204.
15. Salvati, L., III, S.K. Valluri, and D.D. Dlott, From a single grain to microstructure: How explosive grains interact under shock compression. AIP Conference Proceedings, 2023. 2844(1): p. 290010.
16. Bassett, W.P. and D.D. Dlott, Multichannel emission spectrometer for high dynamic range optical pyrometry of shock-driven materials. Review of Scientific Instruments, 2016. 87(10).
17. Johnson, B.P., et al., Observing Hot Spot Formation in Individual Explosive Crystals Under Shock Compression. The Journal of Physical Chemistry A, 2020. 124(23): p. 4646-4653.
18. Bassett, W.P., et al., Shock initiation of explosives: High temperature hot spots explained. Applied Physics Letters, 2017. 111(6).
19. Zhao, S., T.C. Germann, and A. Strachan, Molecular dynamics simulation of dynamical response of perfect and porous Ni/Al nanolaminates under shock loading. Physical Review B, 2007. 76(1): p. 014103.